Additively manufactured lattice structures: An innovative defect-based design methodology against crash impact

Engineering Failure Analysis 152 (2023) 107436

Contents lists available at ScienceDirect

Engineering Failure Analysis

journal homepage: www.elsevier.com/locate/engfailanal

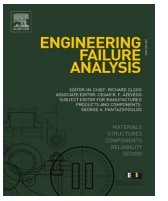

Additively manufactured lattice structures: An innovative defect-based design methodology against crash impact

C. Boursier Niutta *, D.S. Paolino, A. Tridello

Department of Mechanical and Aerospace Engineering, Politecnico di Torino, Corso Duca degli Abruzzi 24, 10129 Torino, Italy

ARTICLE INFO

Keywords:
Additive Manufacturing
Lattice structures
Defect population
Crashworthiness design

ABSTRACT

It is widely known that defects in lattice structures weaken their mechanical response, resulting in premature failure and affecting their energy absorption capability. In this work an experimental–numerical methodology for the identification of the lower bound design curve of lattice structures subjected to quasi-static compressive and impact tests is proposed and validated on an octet truss lattice structure made of an additively manufactured AlSi10Mg alloy. The defect size distribution is assessed through micro computed tomography and retained in a Finite Element Model (FEM) simulating the mechanical tests by a local reduction of the truss diameter. As the location of critical defects affects the mechanical response, simulations are repeated for different random distributions of the defects within the specimen. Results show that the FEM can correctly predict the mechanical behavior of the lattice structure, with the experimental curves comprised within the band of numerical curves. The lower bound design curve to use for the safe design of components can be finally identified through statistical considerations.

1. Introduction

Aiming at reducing the structural weight for a minor environmental impact of transport vehicles, lattice structures have aroused great interest in recent years thanks to their high strength-to-weight ratio [1]. The use of lattice structures in energy absorbers has proven promising for aerospace and automotive components [2]. The diffusion of Additive Manufacturing (AM) technologies, in combination with Topology Optimization (TO) algorithms, has allowed the design of complex geometries whose mechanical performances are enhanced with respect to those of traditionally manufactured components [3–5].

From a structural integrity perspective, the main drawback of AM processes is the consistent and intrinsic formation of random defects [6,7], such as lack of fusion defects, gas porosities, local microstructural variations etc. More specifically, lack of fusion defects form for insufficient energy and are characterized by an irregular morphology. Pores or cluster of pores form for the presence of gas in the building chamber and are characterized by a spherical shape [8]. Microstructural defects include the local microstructural variations induced by the manufacturing process, such as local grain size variations, which affect in turn the local material properties, as shown by Magarò et al. [9]. Finally, we can also retain surface and subsurface defects, which can form during the removal of supporting structures and which can considerably affect the mechanical performance.

Defects are generally variable in size, ranging from 80 μm to 1000 μm [6,7,10], extremely numerous and randomly disposed within the structure. Their presence degrades the mechanical response of lattice structures. In [11], Boniotti et al. have experimentally

* Corresponding author.
E-mail addresses: carlo.boursier@polito.it (C. Boursier Niutta), davide.paolino@polito.it (D.S. Paolino), andrea.tridello@polito.it (A. Tridello).

https://doi.org/10.1016/j.engfailanal.2023.107436
Received 17 May 2023; Received in revised form 27 June 2023; Accepted 27 June 2023
Available online 30 June 2023

measured strain concentrations in correspondence of defects which affect the static and fatigue performance of the lattice structure. Magarò et al. [9] have recently shown that it is necessary to model the as-built structure and to measure local stress–strain curves through micro-indentation to obtain a global numerical response that accurately predicts the experimental force–displacement curve. To assess the defect population, the Authors performed micro-computed tomography (μ-CT) scans of the tested specimens and used three-dimensional elements in a finite element model to replicate the defective structure. The good accuracy of the numerical model showed the consistent influence of local defects and validated the approach, despite the high computational cost of the model.

In the design of energy absorbers, the presence of defects reduces the strength of the structure, resulting in premature failures that in turn strongly affect their energy absorption capability [7,12]. Therefore, the weakening influence of defects must be properly considered for predicting the mechanical behavior of lattice structures. Furthermore, material defectivity is responsible for the response scatter, especially in the post-peak phase, being the location of critical defects a crucial parameter [12]. Indeed, in the design of lattice structures for energy absorption applications, it is crucial to properly model the compressive behavior beyond the elastic limit, while accounting for the scatter of data due to the defect distribution. However, current methodologies for the design of lattice components do not account for the presence of defects or are not computationally sustainable. Typical approaches are based on a reverse engineering procedure which involves a global increment/decrement of the material properties or of the strut diameter in order to replicate the force–displacement experimental curve [13]. These approaches usually require several ineffective iterations and lead to a Finite Element (FE) model of the lattice structure that is not able to account for the experimental scatter due to the material defectivity [12]. For example, the global variation of the strut diameter aims at approximating the strut diameter irregularities, i.e., variations of the local diameter size and of the centroid position [14]. It is worth noticing that, in highly nonlinear phenomena as in crash impacts, contact between the struts is critical for properly evaluating the energy absorption. A global increment/decrement of the strut diameter influences the contact between the struts, anticipating/delaying the occurrence of densification and affecting in turn the energy absorbed by the structure. On the other hand, the global variation of the material plasticity and deformation at failure can lead to misleading interpretations of the energy absorption capability of the structure.

Regarding the computational time, the effort required by 3D modelling techniques is not appropriate for the design of lattice components, although the high details that can be represented through these approaches [9,14]. Smith et al. [15] compared 3D tetra/hexa- and 1D beam elements for modelling the compressive response of lattice structures. They proved that 1D beam elements are also effective to model the quasi-static response of the structure. More recently, Boursier Niutta et al. [16] have successfully adopted 1D beam elements for replicating the compression of lattice structures made of carbon nylon, showing that the model can correctly predict both the peaks-and-valleys and the foam-like crushing behavior. Campoli et al. [17] firstly proposed to account for the strut diameter irregularities in FE beam elements, showing that this approach effectively improves the prediction of the mechanical behavior of lattice structures. More recently, Karamooz Ravari et al. [18] adopted beam elements to model lattice structures and varied the strut diameters according to a normalized frequency of occurrence of the diameters, which was obtained through measurements in several points of the investigated structure. Both the works [17,18] focused on the geometrical variations of the manufactured specimens with respect to the nominal geometry, rather than on the internal defectivity, and did not investigate the effect of the position of the diameter distribution within the structure on the mechanical response, thus not providing guidelines for the design of lattice structures that account for the material defectivity and the geometrical variations.

In this work, an innovative methodology for the design of lattice structures subjected to crash impact is proposed. The methodology aims at identifying an FE model of the lattice structure that accounts for the weakening influence of the material defectivity and the resulting experimental scatter, while limiting the computational effort by adopting 1D beam elements. The identified FE model can be then adopted for the safe design of lattice components. The methodology is validated on octet truss lattice structure specimens made of an AM AlSi10Mg alloy and subjected to both quasi-static compressive and impact tests. The defect size distribution is assessed through μ-CT scans and retained in the FE model of the mechanical tests by a local reduction of the truss diameter. As the location of critical defects affects the mechanical response [12], simulations are repeated for different random distributions of the defects within the specimen and a band of numerical curves is thus obtained and validated with the experimental results. The lower bound curve to be used for the safe design of components is finally identified through statistical considerations.

The work is divided as follows: in Section 2, the geometry and the AM ALSi10Mg alloy used for the lattice specimen are firstly described; thereafter, the methodology is presented by detailing the μ-CT scans, the experimental tests and the FE model with defects. In Section 3, results are discussed by comparing experimental and numerical curves. Finally, in Section 4, the main findings are summarized and conclusions are given.

2. Materials and methods

In this section, characteristics of the AM AlSi10Mg alloy are firstly presented, together with the geometry of the lattice specimens. The methodology, consisting of micro-CT scans for defect identification, quasi-static and impact tests and numerical modelling with defect population, is then described.

2.1. Materials

The investigated lattice structures are produced with an AlSi10Mg Aluminum alloy manufactured by the BeamIT company through the Selective Laser Melting (SLM) technology. Specimens have been subjected to a stress relieve at 200 °C for 2 h. The stress–strain curve of the material for modeling the material behavior in LS-Dyna has been provided by the BeamIT company. Material density, elastic modulus, yield stress, ultimate strength and ultimate strain are reported in Table 1 together with the standard deviations.

The unit cell of the tested specimens is the octet truss lattice structure, already investigated in the previous works [12,16,19]. Each specimen is made of three replicating unit cells in the three orthogonal directions as shown in Fig. 1.

The nominal strut diameter φ_{nom} is 1.5 mm and the length of the unit cell l is 8.5 mm, thus resulting in a cubic specimen of dimensions 25.5x25.5x25.5 mm. Preliminary observations of the manufactured specimens through an optical microscope and a Scanning Electron Microscope (SEM) revealed a consistent undersizing of the actual strut diameter being the mean value equal to 1.32 mm. This value has been considered as the nominal beam diameter for the numerical analyses.

2.2. Methodology for the identification of the lower bound design curve

The methodology here proposed addresses relevant challenges for the design of lattice structures subjected to crash impact. The inherent material defectivity leads to premature failure and increases the variability of the experimental response, thus requiring statistical considerations for the identification of a proper FE model of the unit cell. In addition, the high sensitivity of the material to strain rate must be properly accounted for crash design. Finally, the computational time must be acceptable for the design of components.

The approach that aims at meeting the above mentioned three points is schematically shown in the flow chart of Fig. 2.

Defect population of the tested specimens is firstly assessed through μ-CT scans. The specimens are then subjected to quasi-static compressive and impact tests. In LS-Dyna environment, the tests are replicated by modelling the lattice structure with less computationally expensive 1D beam elements. The defects are inserted by locally varying the strut diameter in accordance with the numerosity assessed through the μ-CT scans, as detailed in Section 2.2.3. The influence of the defect location is accounted for through statistical analyses. In particular, the numerical simulations are repeated by varying the location of flaws and a mean curve and a standard deviation are identified. Finally, in a defect-free model, material parameters are determined to replicate the lower bound curve, e.g., that obtained from the 2.5% confidence bound, thus identifying the FE model to be used for the safe design of components.

2.2.1. μ-CT scans for the identification for the defect distribution

μ-CT scans have been performed in the laboratories of the J-Tech@PoliTO Research Centre of Politecnico di Torino. Three specimens with the investigated lattice structure have been scanned to obtain consistent information on the material defectiveness, focusing on the biggest flaws. Scanning voltage and current intensity have been set to 170 kV and 100 μA, respectively. In order to scan the whole specimen, the distance between the ray source and the specimen has been set to 100 mm and the distance between the source and the detector has been set to 1000 mm, thus leading to a scanning resolution of 20 μm/pixel. 1600 projections have been performed for the reconstruction. In order to limit beam hardening effects, a copper filter of 0.2 mm has been adopted.

The specimen reconstruction has been performed with the VG-Studio Max software. Firstly, the boundaries of the specimen surface have been recognized and all the internal voids, that the software has recognized as not belonging to the material, have been removed. The internal voids can be thus correctly considered in the defect analysis. Fig. 3 shows the 3D reconstruction of a lattice specimen.

In the defect analysis, which focused on the internal defects, i.e., voids and porosities, and not on the geometrical variations with respect to the nominal geometry of the structure, the software investigates the region within the recognized specimen boundaries and compares the grey scale of each pixel with that of the surrounding pixels, thus returning a probability that the investigated region is a defect. The defect size population has been assessed in terms of equivalent defect diameter, calculated from an equivalent sphere with volume equal to the defect volume. The equivalent defect diameters have been grouped into intervals of equal size and the occurrence of each size has been accordingly estimated.

Fig. 4a shows a magnification of one of the biggest defects identified by the software, whose equivalent diameter size was 680 μm, while Fig. 4b shows the histogram of the occurrence of each defect size.

In the μ-CT analyses, the total number of detected defects varied among the specimens and was equal to almost 17,000 on average. It is worth highlighting that the number of detected defects also vary according to the selected probability threshold. The FE model has been then modified according to the determined defect population.

2.2.2. Quasi-static compressive tests and impact tests

Quasi-static compressive tests have been performed on a Zwick Roell Z100 electro-dynamic machine equipped with a load cell of 100 kN. The compressive displacement rate of the top crossbar has been imposed to 1 mm/min. The tests have been performed up to densification. Two replications of the test have been carried out.

Impact tests have been performed on a Instron Fractovis plus 9350 machine. The experimental setup is reported in Fig. 5.

In order to investigate the strain rate sensitivity of the material, tests have been repeated at two different impact velocities, while

Table 1
Material properties of the AlSi10Mg Aluminum alloy.

Property	Value (Std. Dev.)	Unit
Density	2.69 (0.05)	g/cm^3
Young's modulus	76 (5)	GPa
Yield stress	225 (5)	MPa
Ultimate strength	441 (7)	MPa
Ultimate strain	0.040 (0.002)	–

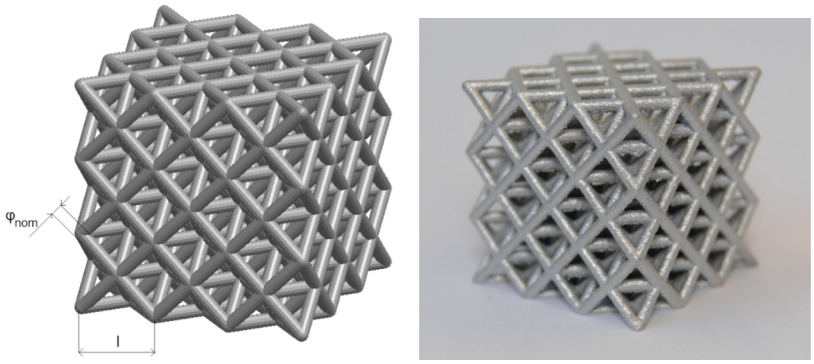

Fig. 1. Lattice structure: a) CAD geometry ($\varphi_{nom} = 1.5$ mm, $l = 8.5$ mm); b) lattice specimen.

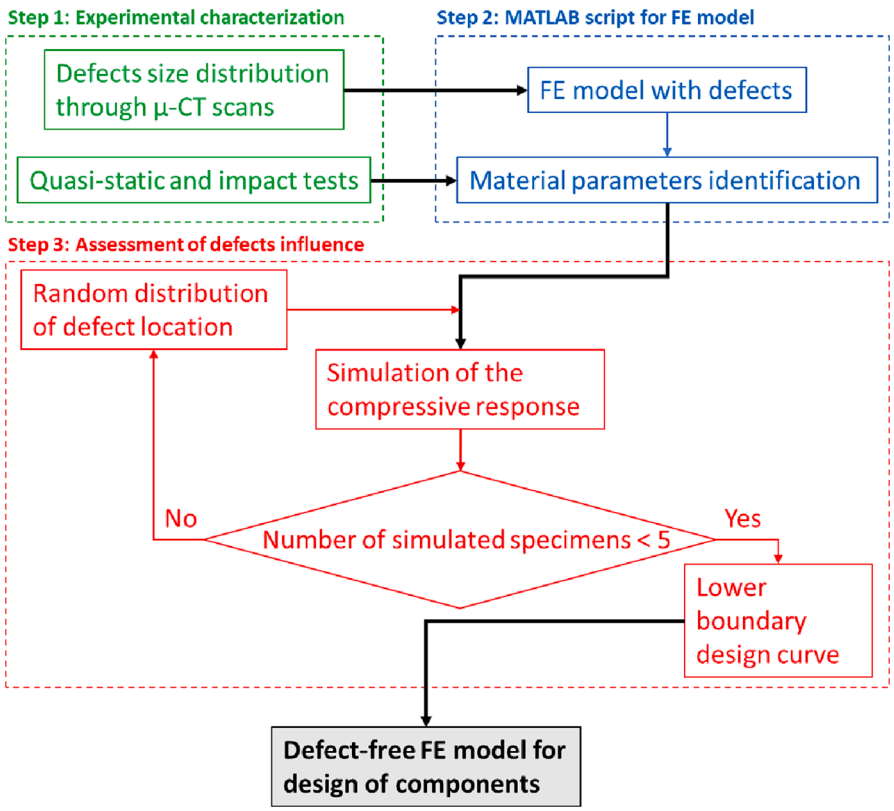

Fig. 2. Flow chart of the proposed methodology.

maintaining the same impact energy of 110 J. The first impact test has been performed at a velocity of 2.0 m/s with total impacting mass of 56.2 kg, while the second test has been performed at a velocity of 2.9 m/s with an impact mass of 26.2 Kg. Two replications for each impact test have been performed.

The load cell positioned above the impactor has acquired the force signal, from which the deceleration has been estimated [20]. Finally, through a double integration in time, the displacement has been calculated [20], thus obtaining the force–displacement curve.

2.2.3. FE model with defect population

The mechanical tests have been modelled in the LS-Dyna environment, performing transient nonlinear FE analyses. To limit the computational effort, 1D Hughes-Liu beam elements have been considered [21]. After a mesh convergence study, the beam length has been set to 1 mm.

μ-CT scans have shown the nonnegligible presence of defects within the structure. In correspondence of these defects, stress

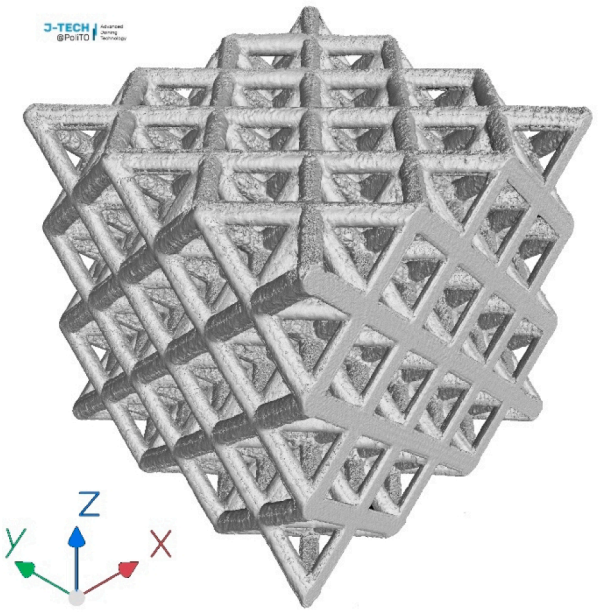

Fig. 3. 3D reconstruction of the lattice structure scanned through μ-CT.

concentrations are expected, which lead to the premature failure of the material [7,11]. In order to capture this effect, a MATLAB script has been created, which modifies the FE model to include the material defectivity.

In particular, the defect population, assessed through the μ-CT scans, has been included in the numerical model by reducing the beam diameter in correspondence of each node according to the defect size, as:

$$\phi_{node} = \phi_{nom} - \phi_{def} \tag{1}$$

being ϕ_{node} the updated node diameter, ϕ_{nom} the nominal beam diameter equal to 1.32 mm and ϕ_{def} the defect size assessed through the μ-CT scans. It is worth highlighting that the formulation of 1D beam elements allows to obtain a stress enhancement that is only a function of the diameter in correspondence of the node and is independent from the mesh size [14,17].

According to the occurrence of each flaw size (see Fig. 4b), the diameter of each node of the FE model has been decreased and defects have been randomly distributed within the FE model. As the total number of the detected defects, i.e., 17,000 on average, and the number of nodes of the discretized model, i.e., 3952, are not equal, the defect population has been included by exploiting the normalized frequency assessed through the μ-CT analyses. In the MATLAB script, the nodes have been randomly listed and the defect diameter has been assigned according to the experimentally assessed frequency of occurrence. In the FE model this is achieved through a dedicated section and by assigning each beam element to a dedicated part. Fig. 6 shows the resulting FE model, where the different colors highlight the parts which each beam element is assigned to.

It is worth highlighting that, by varying the beam diameter, a variation of the material volume is obtained which influences in turn the energy absorption capability of the structure. For this reason, after inserting the defects in the FE model, the material volume has been checked and compared with that provided by the μ-CT analyses, which was equal to 6500 mm^3, resulting in good agreement. In this regard, the mesh size, i.e., the beam length, can also play an important role. For example, once the mesh size has been identified through a mesh convergency study, the beam length can be further decreased to obtain a good agreement with the specimen volume.

Regarding the AlSi10Mg Aluminum alloy behavior, an elasto-plastic material model, i.e., the *MAT_PIECEWISE_LINEAR_PLASTICITY material card [22], has been considered. This material card requires in input also the plastic field of the stress–strain curve, provided by the supplier. Failure of the material, corresponding to element deletion, has been implemented with the *fail* parameter. It is worth remarking that the *fail* parameter is a numerical parameter and does not necessarily correspond to the ultimate strain of the material [22,23]. Accordingly, its value must be identified through comparison with experimental results. The strain rate sensitivity has been accounted for through the well-known Cowper-Symonds model [22,24]:

$$\sigma_y\left(\varepsilon^{pl}, \dot{\varepsilon}^{pl}\right) = \sigma_y^s\left(\varepsilon^{pl}\right)\left[1 + \left(\frac{\dot{\varepsilon}^{pl}}{C}\right)^{\frac{1}{p}}\right] \tag{2}$$

where σ_y^s is the static yield stress, ε^{pl} is the plastic strain, $\dot{\varepsilon}^{pl}$ the plastic strain rate and C and p the Cowper-Symonds parameters to be identified by comparing the experimental and the numerical force–displacement curves.

Contact between the beam elements has been defined with the *CONTACT_AUTOMATIC_GENERAL card which avoids the occurrence of penetration [21].

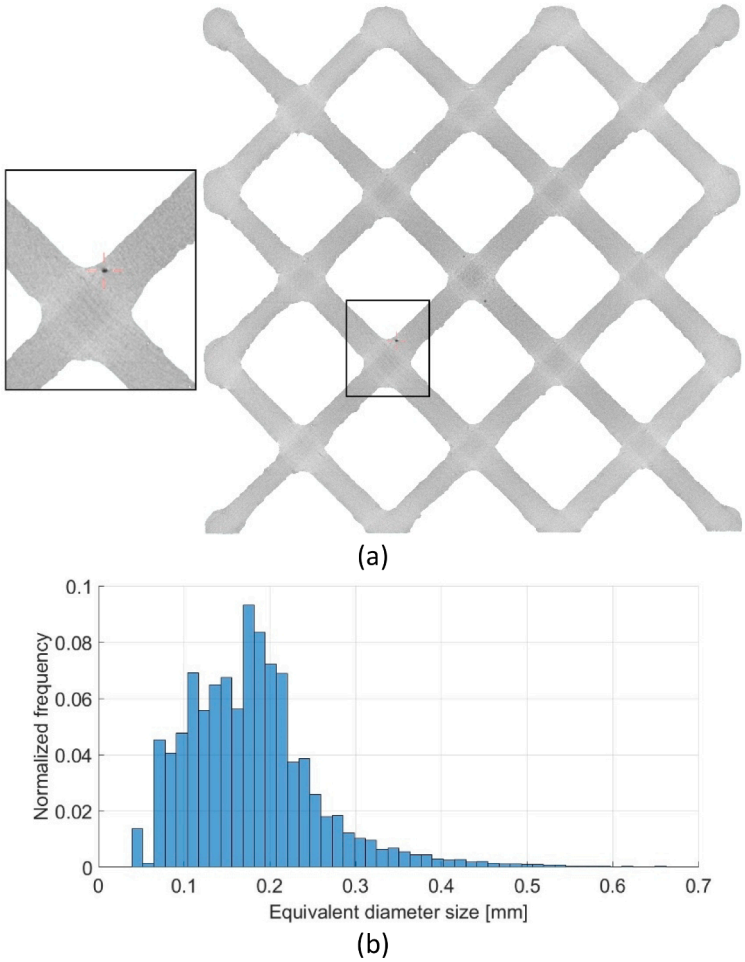

Fig. 4. Results of the defect analyses: a) magnification of a defect of 680 μm; b) occurrence of the defect sizes.

In order to simulate the compressive tests, two rigid walls have been disposed on the upper and lower sides of the specimen. The bottom rigid wall has been fixed, while the upper one moved towards the specimen. In the quasi-static test, the rigid wall moved according to a linear displacement law, while in the impact tests, the experimental mass and initial velocity have been set.

3. Results

In this section, the results of the experimental campaign are firstly presented. Validation of the numerical model which accounts for the defect population is then discussed. Finally, the defect-free FE model which replicates the lower bound curve, i.e., that obtained from the 2.5% confidence bound, is identified.

3.1. Experimental results of the quasi-static and impact tests

In Fig. 7, the experimental force–displacement curves are reported: Fig. 7a shows the quasi-static results, Fig. 7b the impact test at 2.0 m/s, Fig. 7c the impact test at 2.9 m/s and Fig. 7d reports all the results for comparison.

The first quasi-static test has been interrupted after a drop of 70% in the load, while the second test has been conducted until densification occurred. After the peak, the force decreases and the complete fracture is attained. Thereafter, the specimen densifies with the struts sliding one on the other and compacting. As in the densification stage the specimen has not fully fractured, numerical analyses will only focus on the initial phase before the densification occurs.

In the impact tests, oscillations of the force can be observed in the whole crushing event, even though their amplitude decreases. This suggests that these oscillations are not related to a progressive material failure, as will be discussed in the next section. As in the quasi-static tests, in correspondence of the global decrease of the force, the specimen fully fractures and densification initiates. The impact energy is thus absorbed also through a contribution of the densification. As for the quasi-static tests, validation of the numerical model will only focus on the initial phase as in the densification stage the energy is mainly absorbed by sliding friction due to the

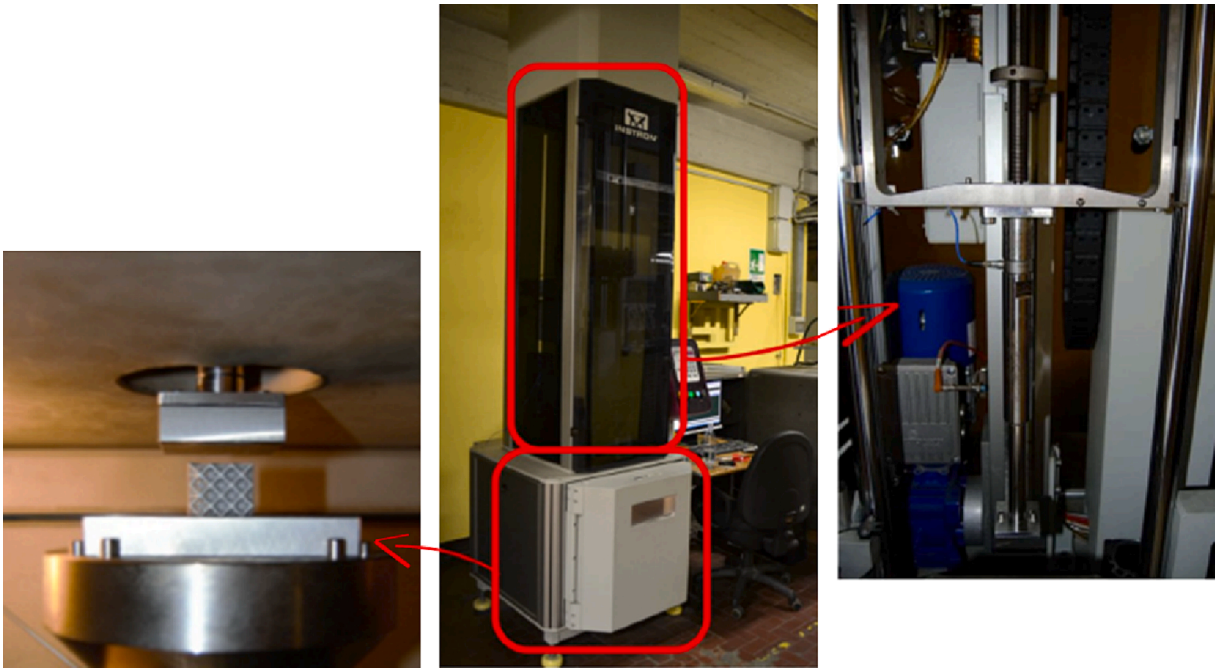

Fig. 5. Experimental setup of the impact tests: the left picture shows the specimen and the impactor, the central picture shows the drop-dart machine and the right figure shows a magnification of the impactor with the load cell positioned above.

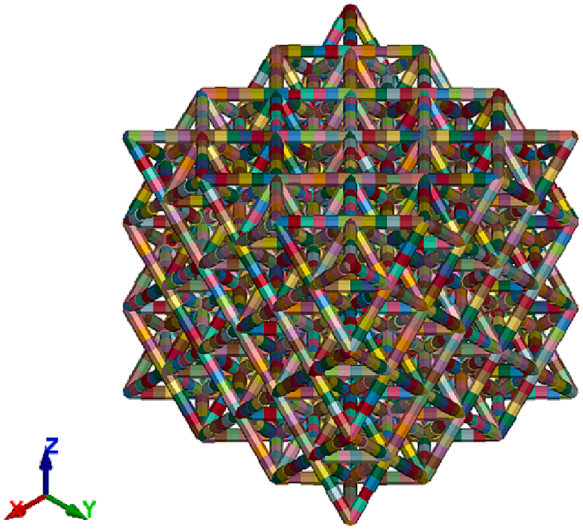

Fig. 6. FE model of the specimen with the experimentally assessed defect population: defects are randomly assigned to the element nodes by reducing the beam diameter.

contact of the crushed beams, which is beyond the interest of the present approach. From the force–displacement curves (Fig. 7d), the strain rate sensitivity can be clearly appreciated, with the maximum force that increases with the strain rate. It is also evident that discrepancies in the response of specimens are not significant in the elastic field and the data scatter increases after the peak force. Indeed, after the peak force, failure initiates in correspondence of the most critical defect and propagates according to defect distribution within the structure.

3.2. Validation of the FE model with defect population

The quasi-static experimental tests have been used to identify the *fail* parameter of the material model, by comparison of the

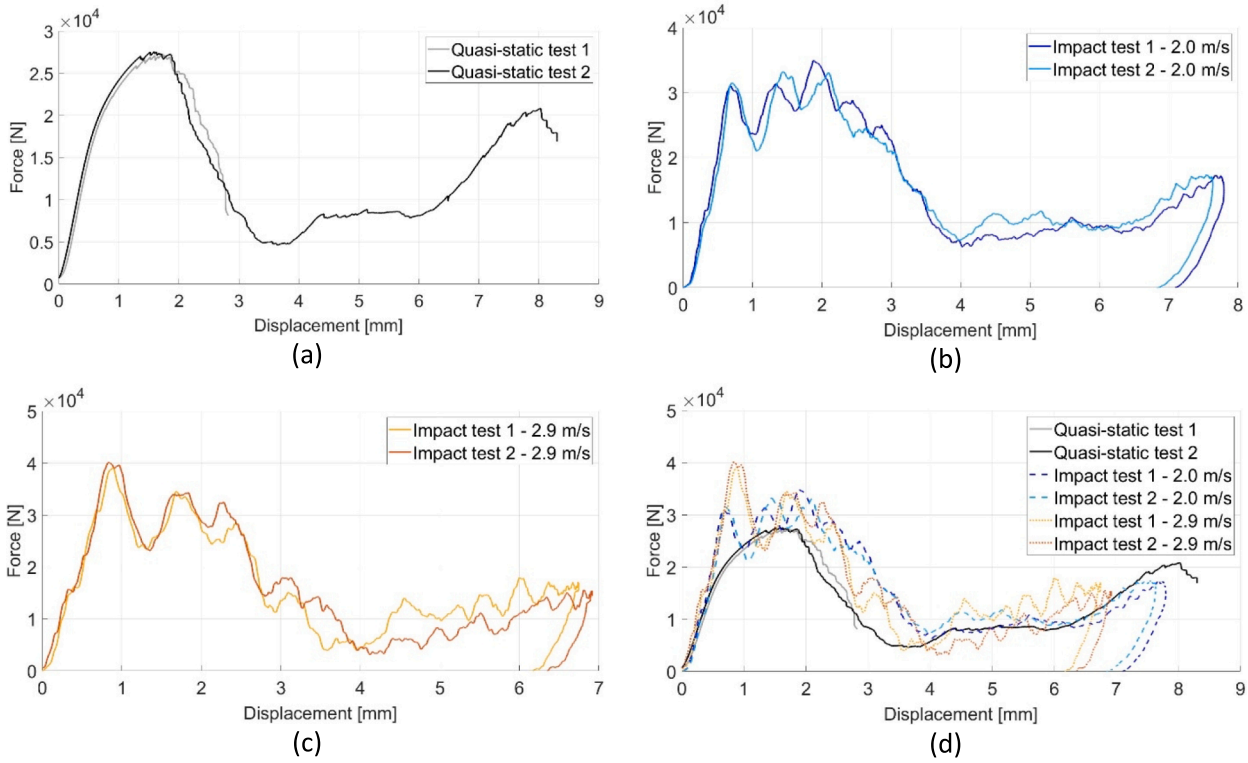

Fig. 7. Force-displacement curves of the tested lattice specimens: a) quasi-static compressive tests; b) impact tests at 2.0 m/s; c) impact tests at 2.9 m/s; d) compassion of all the curves.

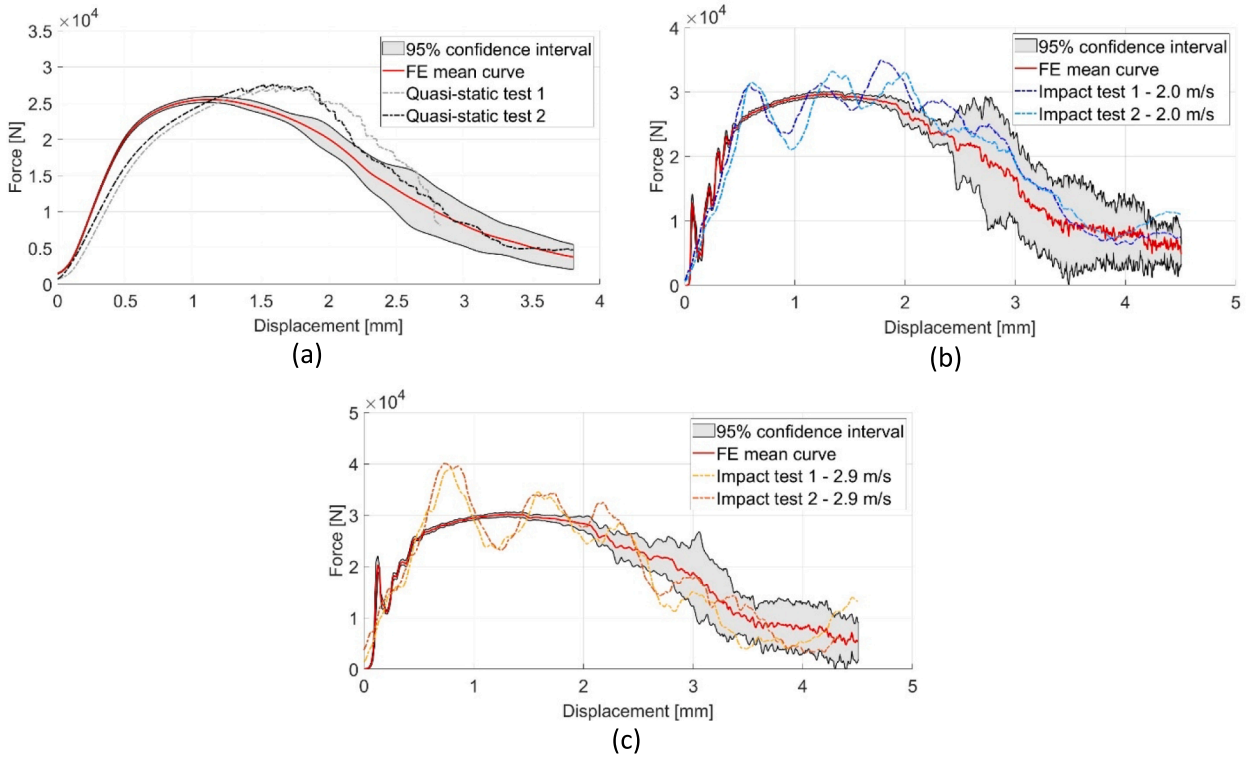

Fig. 8. Comparison of the experimental and numerical results: a) quasi-static compressive tests; b) impact tests at 2.0 m/s; c) impact tests at 2.9 m/s.

experimental and numerical force–displacement curves through a trial-and-error approach. The resulting *fail* parameter is equal to 0.15. Similarly, the parameters C and p of the Cowper-Symonds model have been identified by comparing the experimental and numerical force–displacement curves obtained at the impact velocity of 2.0 m/s. The parameters have been then verified by considering the experimental impact test at 2.9 m/s. The resulting values of C and p are equal to 8500 s^{-1} and 2, respectively.

As the defects distribution affects the mechanical response [12], simulations have been repeated for five different random distributions of the defects within the specimen. A series of force–displacement curves has been thus obtained, from which a mean curve and the related standard deviation can be determined. The mean force–displacement curve has been calculated by averaging the force at each instant of the simulations. Similarly, the standard deviation of the force has been determined at each instant of the simulations. Regarding the displacements, in the quasi-static simulation, the rigid wall displacement law has been considered. In the impact simulations, the displacement has been calculated by double integration of the acceleration, calculated from the averaged force as in the experimental tests [20]. Fig. 8 shows the comparison of the experimental and numerical force–displacement curves, where the numerical mean curve and the band related to the 95% confidence interval are reported. The 95% confidence intervals have been computed from the force repetitions collected at each displacement and by assuming, for the collected data, a Normal distribution. In Fig. 8a, the quasi-static tests are compared, while Fig. 8b and Fig. 8c refer to the impact tests comparison at 2.0 m/s and 2.9 m/s, respectively.

As shown in Fig. 8, the numerical results well replicate the experimental curves, with the numerical mean force–displacement curves in good agreement with the corresponding experimental results. In all the cases, the numerical band well contains the experimental curves in the post-peak phase, when progressive damaging is going on. It can be also appreciated that, in accordance with the experimental results, the numerical curves are practically coincident in the elastic field, i.e., the standard deviation and the band size are extremely limited, while they diverge after the peak force and the band size increases. While the presence of defects is the cause of premature failure, their distribution within the specimen is the governing parameter in the post-peak phase. The dispersion is higher in the impact tests and increases with the strain rate, which is likely due to the increasing contribution of the inertial effects. In this regard, it is worth highlighting that, by reducing the beam diameter to account for the presence of defects according to the methodology here presented, the beam mass is also reduced, thus influencing the inertial response of the beams. Furthermore, the beam diameter reduction delays the contact between the beams, thus affecting the post-peak phase.

Regarding the dispersion of the data, it is also worth noticing that, according to the proposed methodology, the scatter of the results is assessed by performing several numerical simulations where the defect location is randomly modified. By statistically accounting for the effect of the defect location within the structure, the methodology allows to reduce the number of experimental tests required to assess the experimental variability.

In the comparison of the quasi-static tests, it can be observed that the numerical model has a slightly stiffer response than the experimental structures in the elastic regime. In addition, a nonlinear trend before the peak force, which is likely due to an extensive plastic deformation of the structure, is rather pronounced in the experimental curves, while it is less evident in the numerical results. These discrepancies can be attributed to the fact that the material model refers to a tensile stress–strain curve, while most of the struts are subjected to compression. According to [25], where the same Aluminum alloy was tested, tensile and compressive properties, particularly elastic modulus and yield strength, can differ. Furthermore, the struts are differently oriented, and the resulting material properties differ depending on the building direction, as widely shown in the literature [3,26].

In the impact tests, the Finite Element model well replicates the force–displacement responses both at 2.0 m/s and at 2.9 m/s, except for the higher stiffness, as in the quasi-static tests. However, differently from the quasi-static tests, the Finite Element model well replicates the structural behavior even in correspondence of the peak force. This can be explained by considering that, in the dynamic tests, the parameters C and p of the Cowper-Symonds model, which adjust the yield limit of the material according to the strain rate, have been identified. Finally, oscillations in the experimental force can be observed which instead cannot be found in the numerical model. According to the numerical model, the oscillations cannot be attributed to a progressive and local failure of the structure. Rather, these oscillations can be explained by considering the inertial effects of the impactor, which are captured by the load cell, mounted at the top of the impactor, as shown in Fig. 5.

Finally, it is worth highlighting that the quasi-static simulations last about 750 s, while the impact simulations take about 1000 s on a desktop computer with Intel Core i7-8700 (3.2 GHz) and 32 GB of RAM. The computational effort is thus very limited. With respect to 3D solid elements, the 1D beams allows to reduce the computational time of more than one order of magnitude [15]. Smith et el. [15], who investigated the compressive behavior of lattice structures both through 3D elements and through 1D beam elements, showed that the solution of a lattice unit cell modelled with 3D elements lasted 200 s on their machine, while the time required by 1D beam elements of the same size was 10 s on the same machine.

3.3. Identification of the defect-free FE model

The lower bound curves of the 95% confidence intervals, i.e., the 2.5% confidence bounds, have been finally considered for the identification of a defect-free FE model of the structure. The objective is to identify the material parameters that allow replicating the lower bound curve, thus ensuring the safe design through the determined FE model. Furthermore, the defect-free FE model is easier to build with respect to the model with defects and further reduces the computational effort. As the energy absorption capability of a structure is strongly governed by the volume of material involved in the crushing event, it is necessary to guarantee that the defect-free model has the same volume of the tested structures. Therefore, the strut diameter of the defect-free has been reduced from the nominal value of 1.32 mm to 1.10 mm to ensure that the volume of the structure is 6500 mm^3, as assessed through the μ-CT analyses.

As for FE model with defects, the *fail* parameter of the material model has been determined by comparison with the lower bound

curve obtained in the quasi-static tests, while for the parameters C and p of the Cowper-Symonds model the same already identified values, i.e., 8500 s^{-1} for C and 2 for p, have been considered. Indeed, according to the Cowper-Symonds model, the strain rate sensitivity affects the yield strength of the material and is not a function of the defect population. The resulting value of the *fail* parameter is 0.09.

Fig. 9 shows the comparison of the lower bound curve of the band and the defect-free model response. In Fig. 9a, the quasi-static comparison is reported, while Fig. 9b and 9c show the impact responses at 2.0 m/s and 2.9 m/s, respectively.

The defect-free FE model well captures the lower limits in the investigated conditions and, accordingly, can be safely adopted for the design of octet truss lattice components made of AlSi10Mg. However, it is worth remarking that the determined FE model has a uniform beam diameter of 1.10 mm, which is slightly smaller than the actual strut diameter of 1.32 mm assessed through μ-CT analyses. As highlighted in the previous section, a diameter reduction affects both the inertial response of the beams and the contact between the beams, which is delayed in the crushing event. We can therefore state that the FE model can correctly and safely predict the structural behavior in the whole failure process, while it cannot accurately predict the onset of densification, which will likely occur before in the real structure.

Finally, it is worth remarking that the defect-free FE model further reduce the computational effort with respect to standard approaches in the literature [9] and to the model with defects. On the same desktop computer with Intel Core i7-8700 (3.2 GHz) and 32 GB of RAM, the quasi-static simulations last about 600 s, while the impact simulations require 750 s. The proposed modelling approach based on 1D beam elements thus requires feasible computational effort for the design of lattice components against crash, without sacrificing the accuracy.

4. Conclusions

This work presents an innovative methodology for the design of lattice components against crash impact. The methodology accounts for the weakening influence of manufacturing defects, which unavoidably form in Additive Manufacturing (AM) components. Defects lead to the premature failure of the structure and are responsible for the response scatter in the post-peak phase. However, modelling the influence of defects can be computationally unfeasible, especially when designing lattice components for crash applications. The proposed methodology thus aims at accounting for the presence of defects without requiring computationally expensive Finite Elements (FE) models.

The lattice structure is thus modelled with 1D beam elements, in the LS-Dyna environment. By scanning the lattice structure through a micro-computed tomography (μ-CT), the defect size population, i.e., the equivalent diameter size of the defects, can be obtained and retained in the FE model of the structure by reducing the beam diameter at each node according to the assessed defect size. Defects are randomly distributed within the structure according to the experimental occurrence of the defect sizes. The influence of critical defect location is accounted for by repeating the simulations for different distributions of the flaws and a mean response curve, together with the standard deviation, can be determined. This also allows to reduce the number of experimental tests required to assess the experimental variability. Finally, a defect-free FE model which replicates a lower bound curve, e.g., that obtained from the 2.5% confidence bound, thus allowing the safe and computationally sustainable design of lattice components, is identified.

The methodology has been validated on an octet truss lattice structure made of AM AlSi10Mg alloy. Specimens with three repetitions of the unit cell in each direction have been tested under quasi-static and impact compressive tests at 2.0 m/s and 2.9 m/s, thus retaining the material strain rate sensitivity. Results have shown that defects are responsible for the premature failure of the structure and that the response scatter increases in the post-peak phase. By replicating the tests in the LS-Dyna environment with different defect distributions, a series of numerical force–displacement curves have been obtained, from which a mean curve and the related standard deviation can be determined. The band related to the 95% confidence interval has been shown to well contain the experimental results in all loading conditions, with the FE model being capable also to properly replicating the experimental strain rate sensitivity. Also, in accordance with the experimental results, the numerical curves are practically coincident in the elastic field, i.e., the standard deviation and the band size are extremely limited in this region. On the contrary, the numerical curves diverge after the peak force and the band size increases, which suggests that the presence of defects is the cause of premature failure, while their distribution within the specimen is the governing parameter in the post-peak phase. Finally, the defect-free FE model which correctly replicates the lower bound curves and which can be safely adopted for the design of octet truss lattice components made of AlSi10Mg, has been identified. It is worth remarking that the tested lattice structures had the same volume fraction of the material. In case of other relative densities, the defect population should be accordingly identified to apply the proposed methodology, as the defect size distribution can change according to the volume fraction. Furthermore, the defect size distribution can also change with the specimen dimensions, thus leading to a size effect, i.e., the dependence of the mechanical response on the dimensions of the investigated specimen. Extensive investigations on the defect distribution and its variation with the specimen size are required in this regard and represent a further development of the activity.

Declaration of Competing Interest

The authors declare that they have no known competing financial interests or personal relationships that could have appeared to influence the work reported in this paper.

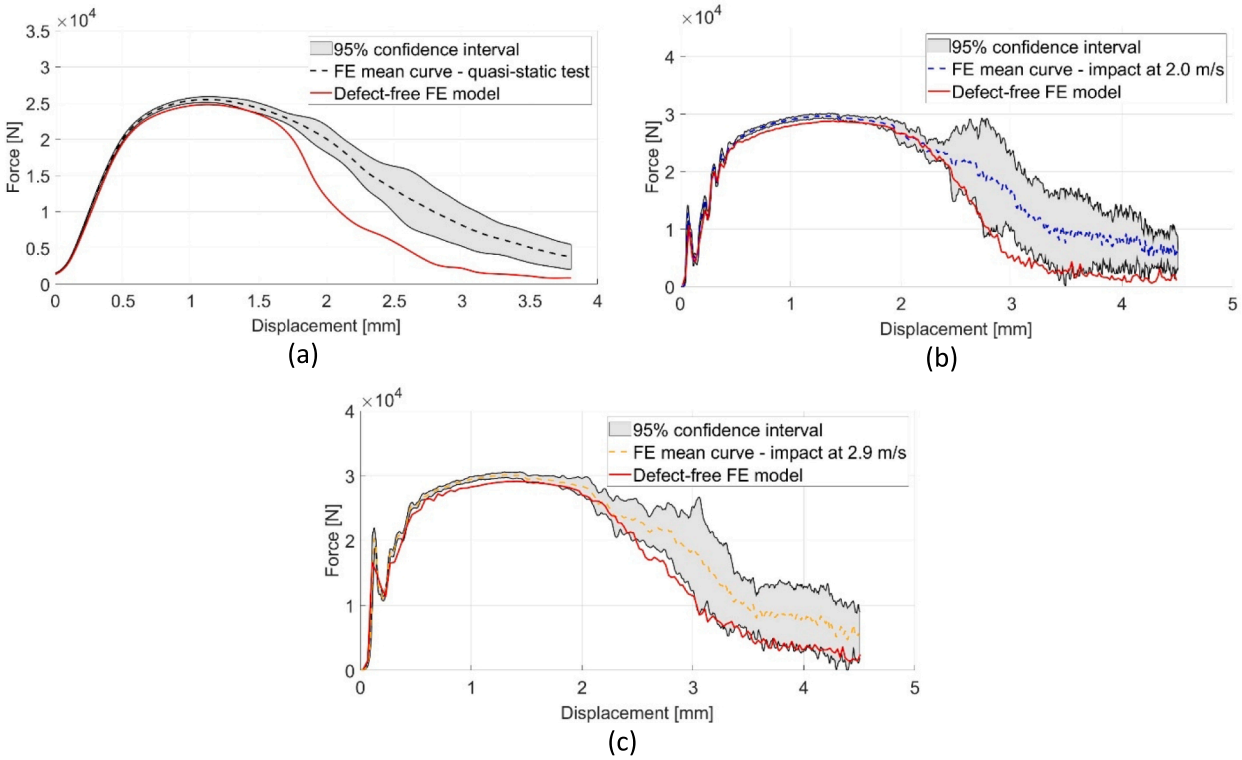

Fig. 9. Identification of the defect-free FE model and approximation of the lower bound curve for a confidence interval of 95%: a) quasi-static compressive tests; b) impact tests at 2.0 m/s; c) impact tests at 2.9 m/s.

Data availability

Data will be made available on request.

References

[1] Z. Ozdemir, E. Hernandez-Nava, A. Tyas, J.A. Warren, S.D. Fay, R. Goodall, et al., Energy absorption in lattice structures in dynamics: Experiments, Int. J. Impact. Eng. 89 (2016) 49–61, https://doi.org/10.1016/j.ijimpeng.2015.10.007.

[2] M.F. Ashby, The properties of foams and lattices, Philos. Trans. R. Soc. A Math. Phys. Eng. Sci. 364 (2006) 15–30, https://doi.org/10.1098/rsta.2005.1678.

[3] F. Tamburrino, S. Graziosi, M. Bordegoni, The design process of additively manufactured mesoscale lattice structures: A review, J. Comput. Inf. Sci. Eng. (2018) 18, https://doi.org/10.1115/1.4040131.

[4] A.A. Zadpoor, Mechanical performance of additively manufactured meta-biomaterials, Acta Biomater. 85 (2019) 41–59, https://doi.org/10.1016/j.actbio.2018.12.038.

[5] T. Maconachie, M. Leary, B. Lozanovski, X. Zhang, M. Qian, O. Faruque, et al., SLM lattice structures: Properties, performance, applications and challenges, Mater. Des. (2019) 183, https://doi.org/10.1016/j.matdes.2019.108137.

[6] N. Sanaei, A. Fatemi, Defects in additive manufactured metals and their effect on fatigue performance: A state-of-the-art review, Prog. Mater. Sci. 117 (2021), 100724, https://doi.org/10.1016/j.pmatsci.2020.100724.

[7] T. Yu, H. Hyer, Y. Sohn, Y. Bai, D. Wu, Structure-property relationship in high strength and lightweight AlSi10Mg microlattices fabricated by selective laser melting, Mater. Des. (2019) 182, https://doi.org/10.1016/j.matdes.2019.108062.

[8] C. Weingarten, D. Buchbinder, N. Pirch, W. Meiners, K. Wissenbach, R. Poprawe, Formation and reduction of hydrogen porosity during selective laser melting of AlSi10Mg, J. Mater. Process Technol. 221 (2015) 112–120, https://doi.org/10.1016/j.jmatprotec.2015.02.013.

[9] P. Magarò, G. Alaimo, M. Carraturo, E. Sgambitterra, C. Maletta, A novel methodology for the prediction of the stress–strain response of laser powder bed fusion lattice structure based on a multi-scale approach, Mater. Sci. Eng. A (2023) 863, https://doi.org/10.1016/j.msea.2022.144526.

[10] A. Tridello, J. Fiocchi, C.A. Biffi, G. Chiandussi, M. Rossetto, A. Tuissi, et al., Effect of microstructure, residual stresses and building orientation on the fatigue response up to 109 cycles of an SLM AlSi10Mg alloy, Int. J. Fatigue 137 (2020), 105659, https://doi.org/10.1016/j.ijfatigue.2020.105659.

[11] L. Boniotti, S. Beretta, S. Foletti, L. Patriarca, Strain concentrations in BCC micro lattices obtained by AM, Proc. Struct. Integr. 7 (2017) 166–173, https://doi.org/10.1016/J.PROSTR.2017.11.074.

[12] N.C. Boursier, R. Ciardiello, F. Berto, D.S. Paolino, A. Tridello, On the influence of Additive Manufacturing defects on the energy absorption capability of a lattice structure, Proc. Struct. Integr. 42 (2022) 1449–1457, https://doi.org/10.1016/J.PROSTR.2022.12.185.

[13] S. Tsopanos, R.A.W. Mines, S. McKown, Y. Shen, W.J. Cantwell, W. Brooks, et al., The influence of processing parameters on the mechanical properties of selectively laser melted stainless steel microlattice structures, J. Manuf. Sci. Eng. 132 (2010) 0410111–04101112, https://doi.org/10.1115/1.4001743.

[14] B. Lozanovski, M. Leary, P. Tran, D. Shidid, M. Qian, P. Choong, et al., Computational modelling of strut defects in SLM manufactured lattice structures, Mater. Des. 171 (2019), 107671, https://doi.org/10.1016/J.MATDES.2019.107671.

[15] M. Smith, Z. Guan, W.J. Cantwell, Finite element modelling of the compressive response of lattice structures manufactured using the selective laser melting technique, Int. J. Mech. Sci. 67 (2013) 28–41, https://doi.org/10.1016/j.ijmecsci.2012.12.004.

[16] C. Boursier Niutta, R. Ciardiello, A. Tridello, Experimental and Numerical Investigation of a Lattice Structure for Energy Absorption: Application to the Design of an Automotive Crash Absorber, Polymers (Basel) 14 (2022) 1116–1137, https://doi.org/10.3390/polym14061116.

[17] G. Campoli, M.S. Borleffs, S. Amin Yavari, R. Wauthle, H. Weinans, A.A. Zadpoor, Mechanical properties of open-cell metallic biomaterials manufactured using additive manufacturing, Mater. Des. 49 (2013) 957–965, https://doi.org/10.1016/J.MATDES.2013.01.071.
[18] M.R. Karamooz Ravari, M. Kadkhodaei, M. Badrossamay, R. Rezaei, Numerical investigation on mechanical properties of cellular lattice structures fabricated by fused deposition modeling, Int. J. Mech. Sci. 88 (2014) 154–161, https://doi.org/10.1016/J.IJMECSCI.2014.08.009.
[19] della Ripa M, Paolino DS, Amorese A, Tridello A. Numerical modelling of the mechanical response of lattice structures produced through AM. Procedia Structural Integrity 2021;33:714–23. https://doi.org/10.1016/J.PROSTR.2021.10.079.
[20] G. Belingardi, M.P. Cavatorta, D.S. Paolino, Repeated impact response of hand lay-up and vacuum infusion thick glass reinforced laminates, Int. J. Impact. Eng. 35 (2008) 609–619, https://doi.org/10.1016/j.ijimpeng.2007.02.005.
[21] LSTC. LS-DYNA Keyword User's Manual Volume I. 2017.
[22] LSTC. LS-DYNA Keyword User's Manual Volume II. 2017. https://doi.org/10.1002/ima.22028.
[23] LSTC. LS-DYNA Keyword User's Manual Volume III. 2017.
[24] Cowper G, Symonds P. Strain hardening and strain-rate effects in the impact loading of cantilever beams. 1957.
[25] E. Sert, L. Hitzler, S. Hafenstein, M. Merkel, E. Werner, A. Öchsner, Tensile and compressive behaviour of additively manufactured AlSi10Mg samples, Prog. Addit. Manuf. 5 (2020) 305–313, https://doi.org/10.1007/s40964-020-00131-9.
[26] G. Dong, Y. Tang, Y.F. Zhao, A survey of modeling of lattice structures fabricated by additive manufacturing, J. Mech. Des. Trans. ASME (2017) 139, https://doi.org/10.1115/1.4037305.